Hector V3.2.0: functionality and performance of a reduced-complexity climate model

Kalyn Dorheim[1], Skylar Gering[2], Robert Gieseke[3], Corinne Hartin[4], Leeya Pressburger[1], Alexey N. Shiklomanov[5], Steven J. Smith[1], Claudia Tebaldi[1], Dawn Woodard[1,6], Ben Bond-Lamberty[1]

1. University Joint Global Change Research Institute, Pacific Northwest National Laboratory, 5825 University Research Ct. #3500, College Park, MD 20740 USA
2. California Institute of Technology 1200 E California Blvd, Pasadena, CA 91125 USA
3. Independent Researcher, Potsdam, Germany
4. Climate Change Division, Office of Atmospheric Protection, U.S. Environmental Protection Agency, Washington, DC, USA
5. NASA Goddard Space Flight Center, 8800 Greenbelt Rd., Greenbelt, MD, 20771 USA
6. Natural Resources Defense Council, 1152 15th St NW #300, Washington, DC 20005 USA

Correspondence to: Kalyn Dorheim (kalyn.dorheim@pnnl.gov)

Abstract. Hector is an open-source reduced complexity climate-carbon cycle model that models critical Earth system processes on a global and annual basis. Here we present an updated version of the model, Hector V3.2.0 (hereafter Hector V3) and document its new features, implementation of new science, and performance. Significant new features include permafrost thaw, a reworked energy balance submodel, and updated parameterizations throughout. Hector V3 results are in good general agreement with historical observations of atmospheric CO_2 concentrations and global mean surface temperature, and its future temperature projections are consistent with more complex Earth System Model output data from the Sixth Coupled Model Intercomparison Project. We show that Hector V3 is a fully open source, flexible, performant, and robust simulator of global climate changes, note its limitations, and discuss future areas of improvement and research with respect to the model's scientific, stakeholder, and educational priorities.

1 Introduction

Reduced complexity climate models (RCMs) fill a critical role within the diverse climate modeling landscape (Sarofim et al., 2021)**.** With strategically simpler representations of large-scale climate processes and dynamics in contrast to coupled Earth System Models (ESMs), RCMs are computationally efficient sources of future climate projections, able to produce large ensembles of results and explore key uncertainties at a fraction of the computational cost of a single ESM run (Kawamiya et

al., 2020). For this reason, RCMs such as Hector, MAGICC, FaIR, and the other Reduced Complexity Intercomparison Project (RCMIP) participating models (Nicholls et al., 2021; Meinshausen et al., 2011; Smith et al., 2018; Nicholls et al., 2020) have been coupled with socioeconomic models (Calvin et al., 2019); used to study climate-carbon interactions and feedbacks (Woodard et al., 2021); supported the assessment of key quantities like global temperature and the carbon budget in various Intergovernmental Panel on Climate Change (IPCC) reports (Smith et al., 2021; Forster et al., 2021); and other applications.

Hector is a globally resolved carbon-climate RCM with explicit terrestrial and ocean carbon cycles as well as active surface ocean chemistry. As a stand-alone climate model, Hector has been used in a variety of other research projects (Woodard et al., 2021; Dorheim et al., 2020; Schwarber et al., 2019; Vega-Westhoff et al., 2019; Pressburger et al., 2023) and participated in the first two phases of RCMIP (Nicholls et al., 2021, 2020). In addition, since 2015, Hector has been the climate component of the Global Change Analysis Model (GCAM) (Calvin et al., 2019) and used to explore the feedback from hydrofluorocarbon emissions from future changes in heating and cooling degree days (Hartin et al., 2021) as well as how carbon dioxide (CO_2) removal technologies may impact the energy-water-land system (Fuhrman et al., 2023).

Since its initial release, model development of Hector has continued in order to reflect the advances made within the climate science and open-source software research communities, and the objective of this paper is to document the latest version of the model. We provide an overview of the model before describing the major changes and upgrades that have been made since Hector V1, focusing on the default model configuration but also describing optional settings. We then compare Hector V3 results with observations and ESM output to examine model performance, and finally discuss future areas of improvement for the model in the context of its goals of accuracy, performance, and broad accessibility.

2 Methods

2.1 Model General Description

The first version of Hector (V1) was described in detail by Hartin et al. (2015). It is a self-contained object-oriented model implemented in C++ with a modular, flexible design. While Hector produces annual output, its adaptive-time solver is capable of operating at a higher frequency to help address issues with numerical instability.

In its default configuration, all Hector runs begin after "spinup" (Thornton and Rosenbloom, 2005), in which the model runs until all carbon pools are in equilibrium; this typically requires ~300 years using the default model parametrization, and typically results in changes of a few percent in the model's major carbon pools. After the spinup phase is complete, the main Hector run begins. A Hector run can either be "free-running" or "constrained." By default, the model is free-running, meaning that its behavior is determined by the time series of emissions and other inputs. During a *constrained* run, the model

60 is forced to match one or more user-prescribed time series. The default free-running model uses time series from 37

61 different emission species and 3 exogenous radiative forcers (see **Supplementary Tables 1**). These emission inputs fall into

62 two categories. The first category consists of emissions that accumulate as greenhouse gas (GHG) concentrations. The GHG

63 concentrations for nitrous oxide (N_2O), methane (CH_4), and 26 halocarbons are calculated using equations that encode a

64 simplified relationship between emissions and concentrations (**Supplementary Tables 3-5**). The GHG concentrations for

65 ozone (O_3) are calculated from interactions between nitrogen oxides (NO_x), carbon monoxide (CO), and non-methane

66 volatile organic compound (NMVOC) emissions (Equations 42-43 in **Supplementary Table 9**). The atmospheric CO_2

67 concentrations are determined in part by the anthropogenic CO_2 emissions (read in as an input) and by the behavior of

68 Hector's terrestrial and ocean carbon cycle components (**Figure 1**). The second category consists of the emissions that

69 impact Hector's radiative forcing budget: carbon monoxide (CO), black carbon (BC), organic carbon (OC), sulfur dioxide

70 (SO_2), and ammonia (NH_3). These emissions are used in equations (**Supplementary Information**) that determine aerosol

71 concentrations and thus radiative forcings. The total radiative forcing is the sum of the forcing effects of all of Hector's

72 atmospheric greenhouse gases, aerosols, and several additional forcing inputs (volcanic forcing, albedo).

73

74 Total radiative forcing is then used to simulate temperature change. Hector's temperature component (Vega-Westhoff et al.,

75 2019) is an implementation of the Diffusion Ocean Energy balance CLIMate model (Kriegler, 2005; Tanaka et al., 2007).

76 DOECLIM is a 1-D pure diffusion ocean model that calculates changes in air temperature 2 meters over ocean/land, sea

77 surface temperature, and within the ocean mixed layer. The sea surface and land surface temperatures from DOECLIM are

78 used by Hector's ocean and land carbon cycles to calculate the carbon fluxes at the next time step. Hector's global mean

79 surface temperature (GMST) is the area-weighted average of these land surface and ocean surface temperatures.

80 **2.2 Changes Since V1**

81 A number of significant architectural, software, and scientific developments have been implemented since the V1 release and

82 documentation manuscript (Hartin et al., 2015). We start by documenting these software changes before discussing other

83 changes and new features affecting Hector's carbon cycle, radiative forcing, temperature calculations, and constrained mode

84 capabilities.

85 **2.2.1 Software**

86 Hector is an open-source community model available on GitHub (https://github.com/jgcri/hector). The repository includes

87 updated project solutions and make files to support building and running Hector from the command line or development

88 environments such as Visual Studio (https://visualstudio.microsoft.com/) or Xcode (https://developer.apple.com/xcode/).

89 Alternatively, users can run Hector as an R (R Core Team, 2021) package, allowing for a broader range of users given R's

90 popularity as a data analysis and simulation tool across many scientific disciplines. The R package wrapper enabled the

development of the Hector User Interface (Pennington and Vernon, 2021), which allows users to run and interact with Hector results in a web browser. Other changes include updated and reduced software dependencies, automated software testing, and auto-generated online documentation. Finally, a Python wrapper Pyhector (Willner et al., 2017) is maintained by community collaborators, broadening the potential users and use cases of the model. The default model remains highly performant: even without any speed optimizations at compile time, running the 550 years (1750-2300) of a standard run takes ~0.5s on a modern laptop. The model is also straightforward to parallelize for large-ensemble analyses (Pressburger et al., 2023). Ultimately, these Hector V3 software changes have led to a more robust, transparent, and accessible community model.

2.2.2 Carbon Cycle

Anthropogenic CO_2 emissions are debited from a geological pool (named "earth" in Hector; cf. **Figure 1**) pool and added to the one-pool, global atmosphere at each timestep. Hector's active carbon cycle is split into terrestrial land and ocean submodels.

As described in detail by Hartin et al. (2015, 2016), Hector's ocean carbon cycle is a four-box module, consisting of two surface-level, intermediate, and deep ocean boxes (**Figure 1**). Carbon and water mass exchange occur between the four boxes respecting simplified representations of advection and thermohaline circulation, with volume transports tuned to approximate a flow of 100 Pg C from the surface high-latitude box to the deep ocean box at steady state, simulating deep water formation. Hector solves for the marine carbonate variables (DIC, pH, alkalinity) with respect to solubility in the two surface layer boxes (Zeebe and Wolf-Gladrow, 2001). The calculation of pCO2 in each surface box is based on the concentration of CO_2 in the ocean and its solubility, in turn a function of temperature, salinity, and pressure. At steady state, the cold high-latitude surface box (> 55° N or S) acts as a sink of carbon from the atmosphere, while the warm low-latitude (≤ 55° N or S) surface box off-gases carbon back to the atmosphere. The ocean-atmosphere flux calculation follows Takahashi et al. (2009). In Hector V3, ocean carbon cycle calculations use sea surface temperature (SST) calculated by DOECLIM (see above), and the preindustrial surface and intermediate/deep ocean carbon cycle pools are initialised from the IPCC sixth assessment report (AR6) Figure 5.12 (Canadell et al., 2021) (see **Table 1**).

Much of the basic functionality of the model's terrestrial carbon cycle is unchanged from the original V1 release (Hartin et al., 2015). Net primary production (NPP) is partitioned into vegetation, detritus, and soil (Figure 1); litterfall moves carbon from vegetation to the soil, and temperature-dependent, first-order decay equations control the heterotrophic release of CO_2 back to the atmosphere from the latter two pools (Hartin et al., 2015). By default, the terrestrial carbon cycle operates as a single, global biome, but Hector can run with an arbitrary number of independent biomes, each with its own set of carbon

pools and parameters; a sample multi-biome parameterization is included with the model's input files, and an example of this was documented in detail by Woodard et al. (2021).

There are also new or changed behaviors in the Hector V3 terrestrial carbon submodel. First, previously land use change (LUC) emissions were specified as a single time series that could be positive or negative, reflecting net emission or uptake, and this value was added (subtracted) to the atmosphere and subtracted (added) from the vegetation, detritus, and soil pools (Hartin et al., 2015). In V3, these are now provided in separate input time series that must be strictly positive and correspond to the gross emissions and uptake fluxes, respectively, and because of how LUC now affects NPP (see below), are assumed to include any regrowth fluxes from previous LUC. A similar change has been made to the fossil fuel/industrial emissions, which are now specified by two gross fluxes of emissions and uptake. This provides users with more flexibility to specify how the gross fluxes result in the net flux, but no behavior change otherwise. Note that the model still accepts net fluxes if that is all that is available, as is the case for the RCMIP Shared Socioeconomic Pathway (SSP) scenarios (Nicholls et al., 2020).

Second, LUC fluxes now affect the land carbon pools in proportion to those pools' size, not via fixed allocation fractions as previously. This is a more conservative assumption than the previous user-defined allocation approach, given the large uncertainty about LUC flux magnitudes and interactive carbon-cycle effects (Yue et al., 2020; Friedlingstein et al., 2023). In addition, in a non-spatial model such as Hector, the carbon pool sizes are governed by the total amount of carbon in the system and the first-order equations linking the pools; LUC loss is only temporary until the pools re-equilibrate. The new approach is thus simpler and in most cases will have only minor effects on model results.

Third, terrestrial NPP is now affected by LUC: the model tracks how much cumulative carbon has been lost (or gained) due to LUC, relative to preindustrial conditions, and then adjusts NPP by this fraction in addition to the pre-existing temperature and CO_2 adjustments to NPP described by Hartin et al. (2015). The logic behind this change is that extensive historical deforestation is known to affect photosynthesis and NPP (Ito, 2011; Malhi et al., 2004; Kaplan et al., 2012), and in previous versions of Hector deforestation did not affect the model's NPP at all. The new behavior is:

$$NPP(t) = NPP_0 \times f(C_{atm}, \beta) \times f(LUC_v) \tag{1}$$

where t is the current timestep; NPP_0 is pre-industrial NPP; and the two f terms represent CO_2 fertilization (Wang et al., 2020) and the aforementioned LUC effect on NPP. This change provides a better match with known LUC effects on terrestrial biomass and production (Winkler et al., 2021; Malhi et al., 2004). More generally, it means that Hector does not regrow vegetation after LUC-driven deforestation; regrowth fluxes should be included in the LUC inputs (see above).

Fourth, Hector V3 also includes a novel implementation of permafrost thaw, a potentially significant process affecting the earth system (Hugelius et al., 2020) that releases both CO_2 and CH_4 into the atmosphere. Hector's permafrost implementation was fully described by Woodard et al. (2021). Briefly, permafrost is treated as a separate land carbon pool that becomes available for decomposition into both CH_4 and CO_2 once thawed (Schädel et al., 2014). The thaw rate is controlled by biome-specific land surface temperature and calibrated to be consistent with both historical data and CMIP6 projections (Burke et al., 2020). Woodard et al. (2021) found that the fraction of thawed permafrost carbon available for decomposition was the most influential parameter in this approach and that adding permafrost thaw to Hector resulted in 0.2–0.25 °C of additional warming over the 21st century. The addition of permafrost to the V3 model produced changes in climate and permafrost carbon pools fully consistent with those reported by Woodard et al (2021).

An optional new feature in Hector V3 is the ability to track the flow of carbon as it moves between the land and ocean carbon pools and the atmosphere (as CO_2). At a user-defined start-tracking date, the model tags all carbon in each of its pools as self-originating—e.g., the soil pool is deemed to be composed of 100% soil-origin carbon. As the model then runs forward, the origin tag is retained as carbon is exchanged between the models' various pools; if 1 Pg C with origin X is incorporated into a 19 Pg C pool with origin Y, for example, at the next timestep, the 20 Pg C pool is tracked as 5% origin X, 95% origin Y. At the end of a run, detailed information about the composition of each pool at each time point can be analyzed. This capability does not affect model behavior or any outputs, although it does impose a substantial performance penalty. Carbon tracking was described in detail by Pressburger et al. (2023) and is off by default.

2.2.3 Radiative Forcing

At each time step, after Hector's carbon cycle solves and all GHG concentrations are computed, Hector calculates total radiative forcing as the sum of 39 forcing effects (listed in **Supplementary Table 1**), each relative to the 1750 base year. The forcing effects for volcanoes and albedo are read in as inputs, as well as a normally-unused "miscellaneous forcing" input available for experimental manipulation. The remaining 36 forcing effects for various aerosols, aerosol-cloud interactions, pollutants, and greenhouse gases are calculated internally within Hector. The forcing effects of tropospheric O_3 and stratospheric H_2O use the same calculations as Hartin et al. (2015). For the other forcing agents, CO_2, CH_4, N_2O, 26 halocarbons, aerosol-cloud interactions, and effects of BC, OC, SO_2, and NH_3, Hector V3 has adopted the forcing equations from AR6 (see **Supplementary Table 5**). Of these, the forcing effect from NH_3 was not previously included in Hector. In addition, the aerosol-cloud interaction forcing replaces the indirect effects of SO_2 forcing that was previously used to approximate the SO_2 and cloud interactions.

2.2.4 Temperature

As of V2, Hector replaced a 0-D energy balance model with DOECLIM (Vega-Westhoff et al., 2019). DOECLIM uses Hector's total radiative forcing to determine global temperature change. DOECLIM is a four-box energy balance model, meaning that it models heat transfer within the climate system represented by four idealized boxes: land (surface), air (2 meters) over land, air (2 meters) over the ocean, and sea surface (ocean mixed layer). DOECLIM uses a system of differential equations to model the temperature change in the four boxes in response to radiative forcing while accounting for the proportional differences in ocean and land masses and effective heat capacity (Tanaka et al., 2007).

In Hector V3, DOECLIM is a fully integrated component of the model, and its outputs now affect Hector's land carbon cycle: DOECLIM's land temperature drives heterotrophic respiration, and sea surface temperature affects ocean carbon cycle dynamics. The difference in land and ocean temperature change, or land-ocean warming ratio, is an emergent property of DOECLIM and is used by default. Two additional parameters can be used to adjust the contributions of aerosols (BC, OC, SO_2, NH_3, and aerosol-cloud interactions) and volcanic forcing to global temperature. By default these are set to a value of one, with the assumption being that the forcing-temperature relationship is consistent for all forcers. These scalar terms allow users to adjust the temperature sensitivity to aerosol and volcanic forcing in uncertainty analyses or when using Hector to emulate ESMs that exhibit different sensitivities to aerosol and volcanic forcings (Dorheim et al. 2020).

2.2.5 Constraints

Hector can run in a "constrained" mode that allows users to overwrite a specified Hector variable with a prescribed time series. Values can be prescribed for atmospheric CO_2 and all other GHG concentrations (effectively resulting in a concentration-forced, not emissions-forced, run). In addition, global temperature, total radiative forcing, and net biome production (effectively turning off the model's terrestrial carbon cycle) can also be constrained. When running in the constrained mode, user-provided values seamlessly overwrite internally-calculated ones, and thus will be used by the downstream Hector components. For example, a Hector run that uses the total total radiative forcing constraint will use the user-prescribed values to calculate energy fluxes and temperature change instead of Hector's internally calculated total ones (see **Table 2** for more examples and details).

The ability to run in the constrained mode is a useful feature that has a number of applications. For example, Hector's concentration constraints enable concentration-forced experiments (e.g., 1% CO_2 and abrupt 4 x CO_2 (Eyring et al., 2016) to comply with the RCMIP protocol (Nicholls et al., 2020). In addition, constraints facilitate coupling Hector with other models: the Net Biome Production (NBP) constraint can be used to pass global NBP value from a regional terrestrial carbon cycle model to Hector, and from there, Hector's ocean carbon cycle and climate dynamics will be calculated. Finally, running Hector in constrained mode can help diagnose model behavior. For example, concentration constraints can be used

214 after a new model development leads to an unexpected increase in global temperature. Running Hector with constrained CO_2

215 concentrations or with total RF will help the developer attribute this novel behavior to changes to Hector's carbon cycle or

216 climate dynamics.

217 **2.2.6 Model Parameterization**

218 Hector's V3 default parameterization is mostly inherited from previous versions of Hector (Hartin et al., 2015; Vega-Westhoff

219 et al., 2019), with the exception of when robust updated estimates are available. In particular, the V3 model uses more recent

220 estimates published for pre-industrial NPP, CO_2, CH_4, and N_2O concentrations, as well as estimates of the pre-industrial carbon

221 cycle to initialize its ocean carbon pools (**Table 1**). Initial pre-industrial sea surface temperatures used by Hector's ocean

222 component were updated from a CMIP5 multi-model mean to a CMIP6 multi-model mean. Historical ocean surface

223 temperature output files from 24 CMIP6 participating models (see **Supplementary Table 10**) were processed to compute the

224 area-weighted mean temperature globally, at both high ($> 55°$) and low ($\leq 55°$) latitudes from 1850 to 1860 (**Table 1**).

225

226 To calibrate the final model, five additional Hector parameters were fit to comparison data using a Nelder-Mead

227 optimization routine (Nelder and Mead, 1965) in a two-part protocol. First, the natural N_2O and CH_4 emissions, which are

228 assumed to be constant throughout the run, were calibrated to median AR6 N_2O and CH_4 radiative forcing (Smith et al.,

229 2018). Second, three Hector parameters—the CO_2 fertilization factor β (unitless), heterotrophic respiration temperature

230 sensitivity Q_{10} (unitless), and ocean heat diffusivity κ ($cm^2 \, s^{-1}$)—were fit to historic CO_2 concentrations (Meinshausen et al.,

231 2017) and GMST (Morice et al., 2021) observations from 1850 to 2021. The Meinshausen et al. (2017) records consist of

232 data for a single year in 1750 and then a complete time series from 1850 to 2014. We chose to use CO_2 and GMST because

233 they are observed data with long time series; conversely, other potential records such as ocean and land sink estimates come

234 from either inversions or models (Friedlingstein et al., 2023). The optimization routine simultaneously minimized the

235 average of the two variables' mean squared errors between Hector CO_2 concentrations and GMST and these observed data.

236 Parameter bounds (i.e., beyond which the optimizer was not allowed) were set at $\pm 2\sigma$, i.e. for a normally-distributed variable

237 ~95% of the possible distribution was used. The best fits for β, Q_{10}, and κ (**Table 1**) were then set as Hector V3's default

238 parameters. The materials and scripts used to calibrate Hector are available in the manuscript repository

239 (https://github.com/JGCRI/Dorheim_etal_2024_GMD) to ensure the reproducibility and transparency of the calibration

240 process.

241 **2.3 Model runs and analysis**

242 To assess model performance, we compared Hector results with both observations and ESM projections. For the historical

243 period, we ran Hector in its default emission-driven mode, with inputs according to the RCMIP protocol (Nicholls et al.,

244 2021, 2020) and the default parameterization described in the previous section. Hector's GMST results from 1850 to 2021

were compared with HadCRUT5 (Morice et al., 2021) GMST observations, while Hector's CO_2 concentrations in the year 1750, and then from 1850 to 2014, were compared with the CMIP6 (Meinshausen et al., 2017) CO_2 concentrations. We used root mean squared error (RMSE) to quantify the differences between model results and the observations. An ordinary least squares linear regression was fit to Hector results and the observational data products to provide additional insights into the goodness of fit. An R^2 value close to one suggests a high degree of correlation between the Hector results and the observations.

For the future period, we first compared Hector's temperature with the AR6 near-term (2021-2024), mid-term (2041-2060), and long-term (2081-2100) warming. For this, Hector was run in emissions-driven mode using the emissions from the RCMIP (Nicholls et al., 2020) protocol. Hector's near-term, mid-term, and long-term warming were computed as the 20-year averages using the model's global mean surface temperature output.

Second, the model was run in a *constrained mode*, in which concentrations for CO_2, CH_4, N_2O, and 26 halocarbons from RCMIP (Nicholls et al., 2020) were prescribed, and compared with CMIP6. These concentration-driven runs were consistent with the CMIP6 protocol (Eyring et al., 2016), allowing for a direct comparison of Hector's climate dynamics with that of the ESMs. For this step, output files from 15 ESMs were processed to compute area-weighted global air, land air, and sea surface temperature anomalies. The CMIP6 models were selected based on data availability for the variables and scenarios; a complete list of models is given in **Supplementary Table 11**. We used the first available ensemble member, since the internal variability between members was unlikely to affect long-term dynamics that are the focus of RCMs (Eyring et al., 2016).

3 Results & Discussion

Hector's historical CO_2 concentrations from an emission-driven run are compared with the Meinshausen et al. (2017) dataset in **Figure 2**. The Hector results closely follow the observed values with a RMSE of 2.14 ppm CO_2 and a correlation coefficient of 0.99, indicating a good agreement between Hector's output and historical carbon cycle observations. **Figure 3** compares emission-driven Hector global mean temperature with historical observations (Morice et al., 2021). The difference between Hector's results and observations is an RMSE of 0.18 °C, which is less than the 0.36 °C standard deviation of the comparison dataset. The linear fit between Hector results and observations has an adjusted R^2 value of 0.87 (**Figure 3**). The recent (2012-2021) decadal average global mean surface temperature for Hector was 0.75 ± 0.09 °C. The model's most notable departure from the observational record is in the late 19th and early 20th centuries (Bauer et al., 2020; Nicholls et al., 2020). The model also generally reproduces modern-day airborne fraction values (Jones et al., 2013; Pressburger et al., 2023). The model's modern (2014-2024) decadal average sea surface temperature and ocean pH are 0.78 ± 0.08 °C and 8.1 ± 0.008, respectively. Hector's land sink for 2013-2022 was 1.94 ± 0.1 Pg C yr^{-1}, which is lower than the land sink of

277   2.9 ± 0.9 Pg C yr^{-1} reported by the Global Carbon Project (GCP, Friedlingstein et al., 2023) during the same decade.

278   Hector's ocean sink of 3.08 ± 0.13 Pg C yr^{-1} is consistent with the GCP ocean sink of 2.8 ± 0.4 Pg C yr^{-1}. Ultimately, we

279   conclude that emission-driven Hector results are in agreement with historical temperature and CO_2 observations except, as

280   noted above, for the latter half of the 19th century.

281

282   The comparison of Hector's historical results with observations is complemented by evaluating Hector's future temperature

283   results against CMIP6 (**Figure 4**) and AR6 assessed warming (Canadell et al., 2021). For the future SSP1-2.6, SSP2-4.5, and

284   SSP5-8.5 projections, Hector's temperature outputs fall squarely within the CMIP6 model spread (**Figure 4**). In addition,

285   **Figure 5** shows Hector's performance in two stylized experiments, 1%CO_2 and 4xCO_2 relative to CMIP6 ESMs. These are

286   baseline experiments of the CMIP DECK protocol (Eyring et al., 2016) designed to diagnose a model's climate sensitivity,

287   feedback strength, provide an idealized benchmark for its transient behavior (for 1%CO_2); and characterize its climate

288   sensitivity and fast-response performance (for 4xCO_2). Again the model falls squarely within the CMIP6 model spread, with

289   no suggestion of anomalous behavior. Hector's transient climate response to cumulative CO_2 emissions is 1.51 °C per 1000

290   Pg C, which is cooler than the IPCC AR6 assessed best estimate of 1.65 °C per 1000 Pg C but falls within the "very likely"

291   range of 1.0 to 2.3 °C per 1000 Pg C (Arias et al., 2021). In general, we conclude that the model exhibits climate responses

292   consistent with AR6 (**Table 3**).

293   **4 Conclusions**

294   In this manuscript, we documented the changes and new features of Hector V3. We showed that emissions-driven Hector's

295   historical results are generally consistent with observed CO_2 concentrations and global mean surface temperature, with the

296   exception of late 19th and early 20th century cooling (Bauer et al., 2020). Hector's future projections of land, ocean, and

297   global average temperature are consistent with a CMIP6 ensemble of models. Thus, we conclude that in the context of

298   RCMs, Hector reproduces most global-scale historical trends and outputs 21st-century projections consistent with Earth

299   system models.

300

301   This fidelity to the current climate and future CMIP6 projections means that there are many potential use cases for Hector,

302   but it is important for users to understand the advantages (as well as disadvantages) in using it relative to other RCMs or

303   ESMs (Nicholls et al., 2021). The freely available R package and online interface facilitate its integration into both standard

304   analytical pipelines as well classroom settings so that students can get hands-on experience with running a climate model and

305   interpreting results; such educational use is supported by the fact that Hector is a well-documented open-source climate

306   model with multiple means of running the model (Hector UI, R Hector, and C++ executable). The model's fully open-source

307   C++ core is easy to couple with other models (Calvin et al., 2019). Using the Hector R package

308   (https://github.com/jgcri/hector), it is easy to generate and analyze large ensembles of Hector results which can be used to

explore uncertainty spaces (Nicholls et al., 2021; Pressburger et al., 2023). Finally, Hector's performance and open, flexible calibration procedure support efforts to emulate more-complex ESMs in support of novel, computationally-intensive experiments (Lu and Ricciuto, 2019; Chen et al., 2023).

It is also important to note Hector's limitations. The model is more complex and thus harder to understand than approaches such as FAIR (Leach et al., 2021), although comparable in complexity to MAGICC (Meinshausen et al., 2011). Hector does not account for the ocean biological pump or changes in ocean stratification; whether these errors are compensating or compounding is unclear and merits future research (Jin et al., 2020). Longer-term simulations are outside of Hector's scope, as is true of most RCMs, as the model's ocean does not include the heat storage changes that strongly affect long-term global temperature dynamics (Baggenstos et al., 2019; Abraham et al., 2013). Future work should aim at understanding/rectifying the differences between Hector's terrestrial carbon sink and other sources while remaining consistent with Hector's moderate complexity and goals; it will always be important to consider trade-offs between costs (i.e., increased complexity threatening interpretability; increased predictive uncertainty from additional model parameters; computational efficiency) and benefits (increased fidelity and representativeness) (Sarofim et al., 2021).

Finally, in addition to continued science improvements, future versions of Hector will benefit from added infrastructure capabilities. First, the current parameter-calibration routine is relatively simple and it may be worth exploring more sophisticated model-calibration procedures (Chen et al., 2023) in future versions of Hector. In addition, a turnkey ability to do probabilistic model forecasts (Fawcett et al., 2015; Ou et al., 2021), i.e. propagating parameter distributions and uncertainty (Pressburger et al., 2023) to produce probabilities of future climate change, is an important capability that a companion R package has been developed to handle (Brown et al., 2024). Leveraging this new capability for probabilistic projects will be important for future analyses using Hector to understand the changing earth and climate system.

Code Availability: Hector V3.2.0 was used to generate the Hector results analyzed and used to generate the figures included in the main text and in the supplementary information. This version of Hector is available at https://github.com/JGCRI/hector at the V3.2.0 release and is archived at https://zenodo.org/records/10698028 this includes all the initialization, emission, and concentration files. All of the code and data used to calibrate Hector, perform all model runs, and produce data visualisations are available at https://github.com/JGCRI/Dorheim_etal_2024_GMD and the GMD3 release associated with this iteration of the manuscript is archived at https://zenodo.org/records/10698650.

Data Availability: All of the calibration, comparison data, and Hector results, along with scripts used to prepare Hector runs analyzed and used to generate the figures included in the main text and in the supplementary information, are available at

339 https://github.com/JGCRI/Dorheim_etal_2024_GMD specifically release GMD3 archived at zendo

340 https://zenodo.org/records/10698650 is the release associated with this iteration of the manuscript.

341 **Author contribution:** KD, BB, SS, SK, RG, CH, LP, AS, and DW all contributed to Hector development. CT and SS

342 helped conceptualize model experiments. KD and BB led the preparation of the original draft and all coauthors contributed

343 to the final draft.

344 **Competing interests:** The authors declare that they have no conflict of interest.

345 **Disclaimer:** The views expressed in this article are those of the authors and do not necessarily represent the views or policies

346 of the U.S. Department of Energy, Environmental Protection Agency, or National Aeronautics and Space Administration.

347 **Acknowledgments:** This research was supported by the U.S. Department of Energy, Office of Science, as part of research in

348 MultiSector Dynamics, Earth and Environmental System Modeling Program. The authors would also like to acknowledge

349 EPA Project DW-089-92459801-8 for contributing to the radiative forcing updates including in Hector v3. The authors

350 would also like to acknowledge Robert Link and Sven Willner for their contributions to Hector and work on Rhector and

351 Pyhector, respectively.

References

353 Abraham, J. P., Baringer, M., Bindoff, N. L., Boyer, T., Cheng, L. J., Church, J. A., Conroy, J. L., Domingues, C. M., Fasullo, J. T.,
354 Gilson, J., Goni, G., Good, S. A., Gorman, J. M., Gouretski, V., Ishii, M., Johnson, G. C., Kizu, S., Lyman, J. M., Macdonald, A. M.,
355 Minkowycz, W. J., Moffitt, S. E., Palmer, M. D., Piola, A. R., Reseghetti, F., Schuckmann, K., Trenberth, K. E., Velicogna, I., and Willis,
356 J. K.: A review of global ocean temperature observations: Implications for ocean heat content estimates and climate change, Rev.
357 Geophys., 51, 450–483, 2013.

358 Arias, P. A., Bellouin, N., Coppola, E., Jones, R. G., Krinner, G., Marotzke, J., Naik, V., Palmer, M. D., Plattner, G.-K., Rogelj, J., Rojas,
359 M., Sillmann, J., Storelvmo, T., Thorne, P. W., Trewin, B., Achuta Rao, K., Adhikary, B., Allan, R. P., Armour, K., Bala, G., Barimalala,
360 R., Berger, S., Canadell, J. G., Cassou, C., Cherchi, A., Collins, W., Collins, W. D., Connors, S. L., Corti, S., Cruz, F., Dentener, F. J.,
361 Dereczynski, C., Di Luca, A., Diongue Niang, A., Doblas-Reyes, F. J., Dosio, A., Douville, H., Engelbrecht, F., Eyring, V., Fischer, E.,
362 Forster, P., Fox-Kemper, B., Fuglestvedt, J. S., Fyfe, J. C., Gillett, N. P., Goldfarb, L., Gorodetskaya, I., Gutierrez, J. M., Hamdi, R.,
363 Hawkins, E., Hewitt, H. T., Hope, P., Islam, A. S., Jones, C., Kaufman, D. S., Kopp, R. E., Kosaka, Y., Kossin, J., Krakovska, S., Lee, J.-
364 Y., Li, J., Mauritsen, T., Maycock, T. K., Meinshausen, M., Min, S.-K., Monteiro, P. M. S., Ngo-Duc, T., Otto, F., Pinto, I., Pirani, A.,
365 Raghavan, K., Ranasinghe, R., Ruane, A. C., Ruiz, L., Sallée, J.-B., Samset, B. H., Sathyendranath, S., Seneviratne, S. I., Sörensson, A.
366 A., Szopa, S., Takayabu, I., Tréguier, A.-M., van den Hurk, B., Vautard, R., von Schuckmann, K., Zaehle, S., Zhang, X., and Zickfeld, K.:
367 Technical Summary, in: Climate Change 2021: The Physical Science Basis. Contribution of Working Group I to the Sixth Assessment
368 Report of the Intergovernmental Panel on Climate Change, edited by: Masson-Delmotte, V., Zhai, P., Pirani, A., Connors, S. L., Péan, C.,
369 Berger, S., Caud, N., Chen, Y., Goldfarb, L., Gomis, M. I., Huang, M., Leitzell, K., Lonnoy, E., Matthews, J. B. R., Maycock, T. K.,
370 Waterfield, T., Yelekçi, O., Yu, R., and Zhou, B., Cambridge University Press, Cambridge, United Kingdom and New York, NY, USA,
371 33−144, 2021.

372 Baggenstos, D., Häberli, M., Schmitt, J., Shackleton, S. A., Birner, B., Severinghaus, J. P., Kellerhals, T., and Fischer, H.: Earth's radiative
373 imbalance from the Last Glacial Maximum to the present, Proceedings of the National Academy of Sciences, 116, 14881–14886, 2019.

374 Bauer, S. E., Tsigaridis, K., Faluvegi, G., Kelley, M., Lo, K. K., Miller, R. L., Nazarenko, L., Schmidt, G. A., and Wu, J.: Historical

375 (1850–2014) aerosol evolution and role on climate forcing using the GISS ModelE2.1 contribution to CMIP6, J. Adv. Model. Earth Syst.,
376 12, https://doi.org/10.1029/2019ms001978, 2020.

377 Brown, J., Smith, S., Tebaldi, C., Pressburger, L., Dorheim, K., and Bond-Lamberty, B.: Matilda v1.0: An R package for probabilistic
378 climate projections using a reduced complexity climate model, PLOS Climate, in press, 2024.

379 Burke, E. J., Zhang, Y., and Krinner, G.: Evaluating permafrost physics in the Coupled Model Intercomparison Project 6 (CMIP6) models
380 and their sensitivity to climate change, Cryosphere, 14, 3155–3174, 2020.

381 Calvin, K., Patel, P., Clarke, L., Asrar, G., Bond-Lamberty, B., Cui, R. Y., Vittorio, A. D., Dorheim, K., Edmonds, J., Hartin, C., and
382 Others: GCAM v5. 1: representing the linkages between energy, water, land, climate, and economic systems, Geoscientific Model
383 Development, 12, 677–698, 2019.

384 Canadell, J. G., Monteiro, P. M. S., Costa, M. H., Cotrim da Cunha, L., Cox, P. M., Eliseev, A. V., Henson, S., Ishii, M., Jaccard, S.,
385 Koven, C., Lohila, A., Patra, P. K., Piao, S., Rogelj, J., Syampungani, S., Zaehle, S., and Zickfeld, K.: Global Carbon and other
386 Biogeochemical Cycles and Feedbacks, in: Climate Change 2021: The Physical Science Basis. Contribution of Working Group I to the
387 Sixth Assessment Report of the Intergovernmental Panel on Climate Change, edited by: Masson-Delmotte, V., Zhai, P., Pirani, A.,
388 Connors, S. L., Péan, C., Berger, S., Caud, N., Chen, Y., Goldfarb, L., Gomis, M. I., Huang, M., Leitzell, K., Lonnoy, E., Matthews, J. B.
389 R., Maycock, T. K., Waterfield, T., Yelekçi, O., Yu, R., and Zhou, B., Cambridge University Press, Cambridge, United Kingdom and New
390 York, NY, USA, 673–816, 2021.

391 Chen, M., Qian, Z., Boers, N., Jakeman, A. J., Kettner, A. J., Brandt, M., Kwan, M.-P., Batty, M., Li, W., Zhu, R., Luo, W., Ames, D. P.,
392 Barton, C. M., Cuddy, S. M., Koirala, S., Zhang, F., Ratti, C., Liu, J., Zhong, T., Liu, J., Wen, Y., Yue, S., Zhu, Z., Zhang, Z., Sun, Z., Lin,
393 J., Ma, Z., He, Y., Xu, K., Zhang, C., Lin, H., and Lü, G.: Iterative integration of deep learning in hybrid Earth surface system modelling,
394 Nature Reviews Earth & Environment, 4, 568–581, 2023.

395 Dorheim, K., Link, R., Hartin, C., Kravitz, B., and Snyder, A.: Calibrating Simple Climate Models to Individual Earth System Models:
396 Lessons Learned From Calibrating Hector, Life Support Biosph. Sci., 7, e2019EA000980, 2020.

397 Eyring, V., Bony, S., Meehl, G. A., Senior, C. A., Stevens, B., Stouffer, R. J., and Taylor, K. E.: Overview of the Coupled Model
398 Intercomparison Project Phase 6 (CMIP6) experimental design and organization, Geosci. Model Dev., 9, 1937–1958, 2016.

399 Fawcett, A. A., Iyer, G. C., Clarke, L. E., Edmonds, J. A., Hultman, N. E., McJeon, H. C., Rogelj, J., Schuler, R., Alsalam, J., Asrar, G. R.,
400 Creason, J., Jeong, M., McFarland, J., Mundra, A., and Shi, W.: CLIMATE POLICY. Can Paris pledges avert severe climate change?,
401 Science, 350, 1168–1169, 2015.

402 Forster, P., Storelvmo, T., Armour, K., Collins, W., Dufresne, J.-L., Frame, D., Lunt, D. J., Mauritsen, T., Palmer, M. D., Watanabe, M.,
403 Wild, M., and Zhang, H.: The Earth's Energy Budget, Climate Feedbacks, and Climate Sensitivity, in: Climate Change 2021: The Physical
404 Science Basis. Contribution of Working Group I to the Sixth Assessment Report of the Intergovernmental Panel on Climate Change,
405 edited by: Masson-Delmotte, V., Zhai, P., Pirani, A., Connors, S. L., Péan, C., Berger, S., Caud, N., Chen, Y., Goldfarb, L., Gomis, M. I.,
406 Huang, M., Leitzell, K., Lonnoy, E., Matthews, J. B. R., Maycock, T. K., Waterfield, T., Yelekçi, O., Yu, R., and Zhou, B., Cambridge
407 University Press, Cambridge, United Kingdom and New York, NY, USA, 923–1054, 2021.

408 Friedlingstein, P., Jones, M. W., Andrew, R. M., Bakker, D. C. E., Hauck, J., Landschützer, P., Le Quéré, C., Luijkx, I. T., Peters, G. P.,
409 Peters, W., Pongratz, J., Schwingshackl, C., Sitch, S., Canadell, J. G., Ciais, P., Jackson, R. B., Alin, S. R., Anthoni, P., Barbero, L., Bates,
410 N. R., Becker, M., Bellouin, N., Decharme, B., Bopp, L., Brasika, I. B. M., Cadule, P., Chamberlain, M. A., Chandra, N., Chau, T.-T.-T.,
411 Chevallier, F., Chini, L. P., Cronin, M., Dou, X., Enyo, K., Evans, W., Falk, S., Feely, R. A., Feng, L., Ford, D. J., Gasser, T., Ghattas, J.,
412 Gkritzalis, T., Grassi, G., Gregor, L., Gruber, N., Gürses, Ö., Harris, I., Hefner, M., Heinke, J., Houghton, R. A., Hurtt, G. C., Iida, Y.,
413 Ilyina, T., Jacobson, A. R., Jain, A., Jarníková, T., Jersild, A., Jiang, F., Jin, Z., Joos, F., Kato, E., Keeling, R. F., Kennedy, D., Klein
414 Goldewijk, K., Knauer, J., Korsbakken, J. I., Körtzinger, A., Lan, X., Lefèvre, N., Li, H., Liu, J., Liu, Z., Ma, L., Marland, G., Mayot, N.,
415 McGuire, P. C., McKinley, G. A., Meyer, G., Morgan, E. J., Munro, D. R., Nakaoka, S.-I., Niwa, Y., Olsen, A., Omar, A. M., Ono, T.,
416 Paulsen, M., Pierrot, D., Pocock, K., Poulter, B., Powis, C. M., Rehder, G., Resplandy, L., Robertson, E., Rödenbeck, C., Rosan, T. M.,
417 Schwinger, J., Séférian, R., Smallman, T. L., Smith, S. M., et al.: Global Carbon Budget 2023, Earth System Science Data, 15, 5301–5369,
418 2023.

419 Fuhrman, J., Bergero, C., Weber, M., Monteith, S., Wang, F. M., Clarens, A. F., Doney, S. C., Shobe, W., and McJeon, H.: Diverse carbon
420 dioxide removal approaches could reduce impacts on the energy–water–land system, Nat. Clim. Chang., 13, 341–350, 2023.

Hartin, C., Link, R., Patel, P., Mundra, A., Horowitz, R., Dorheim, K., and Clarke, L.: Integrated modeling of human-earth system interactions: An application of GCAM-fusion, Energy Econ., 103, 105566, 2021.

Hartin, C. A., Patel, P., Schwarber, A., Link, R. P., and Bond-Lamberty, B. P.: A simple object-oriented and open-source model for scientific and policy analyses of the global climate system – Hector v1.0, Geoscientific Model Development, 8, 939–955, 2015.

Hartin, C. A., Bond-Lamberty, B., Patel, P., and Mundra, A.: Ocean acidification over the next three centuries using a simple global climate carbon-cycle model: projections and sensitivities, Biogeosciences, 4329–4342, 2016.

Hugelius, G., Loisel, J., Chadburn, S., Jackson, R. B., Jones, M., MacDonald, G., Marushchak, M., Olefeldt, D., Packalen, M., Siewert, M. B., Treat, C., Turetsky, M., Voigt, C., and Yu, Z.: Large stocks of peatland carbon and nitrogen are vulnerable to permafrost thaw, Proc. Natl. Acad. Sci. U. S. A., https://doi.org/10.1073/pnas.1916387117, 2020.

Ito, A.: A historical meta-analysis of global terrestrial net primary productivity: Are estimates converging?, Glob. Chang. Biol., 17, 3161–3175, 2011.

Jin, D., Hoagland, P., and Buesseler, K. O.: The value of scientific research on the ocean's biological carbon pump, Sci. Total Environ., 749, 141357, 2020.

Jones, C. D., Robertson, E., Arora, V., Friedlingstein, P., Shevliakova, E., Bopp, L., Brovkin, V., Hajima, T., Kato, E., Kawamiya, M., Liddicoat, S., Lindsay, K., Reick, C. H., Roelandt, C., Segschneider, J., and Tjiputra, J.: Twenty-first-century compatible CO2 emissions and airborne fraction simulated by CMIP5 earth system models under four representative concentration pathways, J. Clim., 26, 4398–4413, 2013.

Kaplan, J. O., Krumhardt, K. M., and Zimmerman, N. E.: The effects of land use and climate change on the carbon cycle of Europe over the past 500 years, Glob. Chang. Biol., 18, 902–914, 2012.

Kawamiya, M., Hajima, T., Tachiiri, K., Watanabe, S., and Yokohata, T.: Two decades of Earth system modeling with an emphasis on Model for Interdisciplinary Research on Climate (MIROC), Progress in Earth and Planetary Science, 7, 1–13, 2020.

Kriegler, E.: Imprecise probability analysis for integrated assessment of climate change, Verlag nicht ermittelbar, 2005.

Leach, N. J., Jenkins, S., Nicholls, Z., Smith, C. J., Lynch, J., Cain, M., Walsh, T., Wu, B., Tsutsui, J., and Allen, M. R.: FaIRv2.0.0: a generalized impulse response model for climate uncertainty and future scenario exploration, Geosci. Model Dev., 14, 3007–3036, 2021.

Lu, D. and Ricciuto, D.: Efficient surrogate modeling methods for large-scale Earth system models based on machine-learning techniques, Geoscientific Model Development, 12, 1791–1807, 2019.

Malhi, Y., Phillips, O. L., Cramer, W., Bondeau, A., Schaphoff, S., Lucht, W., Smith, B., and Sitch, S.: Tropical forests and the global carbon cycle: impacts of atmospheric carbon dioxide, climate change and rate of deforestation, Philos. Trans. R. Soc. Lond. B Biol. Sci., 359, 331–343, 2004.

Meinshausen, M., Raper, S. C. B., and Wigley, T. M. L.: Emulating coupled atmosphere-ocean and carbon cycle models with a simpler model, MAGICC6 – Part 1: Model description and calibration, Atmos. Chem. Phys., 11, 1417–1456, 2011.

Meinshausen, M., Vogel, E., Nauels, A., Lorbacher, K., Meinshausen, N., Etheridge, D. M., Fraser, P. J., Montzka, S. A., Rayner, P. J., Trudinger, C. M., Krummel, P. B., Beyerle, U., Canadell, J. G., Daniel, J. S., Enting, I. G., Law, R. M., Lunder, C. R., O'Doherty, S., Prinn, R. G., Reimann, S., Rubino, M., Velders, G. J. M., Vollmer, M. K., Wang, R. H. J., and Weiss, R.: Historical greenhouse gas concentrations for climate modelling (CMIP6), Geoscientific Model Development, 10, 2057–2116, 2017.

Morice, C. P., Kennedy, J. J., Rayner, N. A., Winn, J. P., Hogan, E., Killick, R. E., Dunn, R. J. H., Osborn, T. J., Jones, P. D., and Simpson, I. R.: An updated assessment of near-surface temperature change from 1850: The HadCRUT5 data set, J. Geophys. Res., 126, https://doi.org/10.1029/2019jd032361, 2021.

Nelder, J. A. and Mead, R.: A simplex method for function minimization, Comput. J., 7, 308–313, 1965.

Nicholls, Z., Meinshausen, M., Lewis, J., Corradi, M. R., Dorheim, K., Gasser, T., Gieseke, R., Hope, A. P., Leach, N. J., McBride, L. A., Quilcaille, Y., Rogelj, J., Salawitch, R. J., Samset, B. H., Sandstad, M., Shiklomanov, A., Skeie, R. B., Smith, C. J., Smith, S. J., Su, X.,

462 Tsutsui, J., Vega-Westhoff, B., and Woodard, D. L.: Reduced Complexity Model Intercomparison Project Phase 2: Synthesizing Earth
463 System Knowledge for Probabilistic Climate Projections, Earths Future, 9, e2020EF001900, 2021.

464 Nicholls, Z. R. J., Meinshausen, M., Lewis, J., Gieseke, R., Dommenget, D., Dorheim, K., Fan, C.-S., Fuglestvedt, J. S., Gasser, T.,
465 Golüke, U., Goodwin, P., Hartin, C., Hope, A. P., Kriegler, E., Leach, N. J., Marchegiani, D., McBride, L. A., Quilcaille, Y., Rogelj, J.,
466 Salawitch, R. J., Samset, B. H., Sandstad, M., Shiklomanov, A. N., Skeie, R. B., Smith, C. J., Smith, S., Tanaka, K., Tsutsui, J., and Xie,
467 Z.: Reduced Complexity Model Intercomparison Project Phase 1: introduction and evaluation of global-mean temperature response,
468 Geosci. Model Dev., 13, 5175–5190, 2020.

469 Nijsse, F. J. M. M., Cox, P. M., and Williamson, M. S.: Emergent constraints on transient climate response (TCR) and equilibrium climate
470 sensitivity (ECS) from historical warming in CMIP5 and CMIP6 models, Earth Syst. Dyn., 11, 737–750, 2020.

471 Ou, Y., Iyer, G., Clarke, L., Edmonds, J., Fawcett, A. A., Hultman, N., McFarland, J. R., Binsted, M., Cui, R., Fyson, C., Geiges, A.,
472 Gonzales-Zuñiga, S., Gidden, M. J., Höhne, N., Jeffery, L., Kuramochi, T., Lewis, J., Meinshausen, M., Nicholls, Z., Patel, P., Ragnauth,
473 S., Rogelj, J., Waldhoff, S., Yu, S., and McJeon, H.: Can updated climate pledges limit warming well below 2°C?, Science, 374, 693–695,
474 2021.

475 Pennington, S. and Vernon, C.: HectorUI: An Interactive Climate Model, IN33B–05, 2021.

476 Pressburger, L. and Dorheim, K. R.: JGCRI/hector_cmip6data: v1.0, https://doi.org/10.5281/zenodo.7304553, 2022.

477 Pressburger, L., Dorheim, K., Keenan, T., McJeon, H., Smith, S., and Bond-Lamberty, B.: Quantifying airborne fraction trends and the
478 destination of anthropogenic CO2 by tracking carbon flows in a simple climate model, Environ. Res. Lett., in press, 2023.

479 R Core Team: R: A Language and Environment for Statistical Computing v4.1.0, R Foundation for Statistical Computing, Vienna, Austria,
480 2021.

481 Sarofim, M. C., Smith, J. B., St Juliana, A., and Hartin, C.: Improving reduced complexity model assessment and usability, Nat. Clim.
482 Chang., 11, 1–3, 2021.

483 Schädel, C., Schuur, E. A. G., Bracho, R., Elberling, B., Knoblauch, C., Lee, H., Luo, Y., Shaver, G. R., and Turetsky, M. R.: Circumpolar
484 assessment of permafrost C quality and its vulnerability over time using long-term incubation data, Glob. Chang. Biol., 20, 641–652, 2014.

485 Schwarber, A. K., Smith, S. J., Hartin, C. A., Vega-Westhoff, B. A., and Sriver, R.: Evaluating climate emulation: fundamental impulse
486 testing of simple climate models, Earth Syst. Dynam., 10, 729–739, 2019.

487 Smith, C., Nicholls, Z. R. J., Armour, K., Collins, W., Forster, P., Meinshausen, M., Palmer, M. D., and Watanabe, M.: The Earth's
488 Energy Budget, Climate Feedbacks, and Climate Sensitivity Supplementary Material, in: Climate Change 2021: The Physical Science
489 Basis. Contribution of Working Group I to the Sixth Assessment Report of the Intergovernmental Panel on Climate Change, edited by:
490 Masson-Delmotte, V., Zhai, P., Pirani, A., Connors, S. L., Péan, C., Berger, S., Caud, N., Chen, Y., Goldfarb, L., Gomis, M. I., Huang, M.,
491 Leitzell, K., Lonnoy, E., Matthews, J. B. R., Maycock, T. K., Waterfield, T., Yelekçi, O., Yu, R., and Zhou, B., 2021.

492 Smith, C. J., Kramer, R. J., Myhre, G., Forster, P. M., Soden, B. J., Andrews, T., Boucher, O., Faluvegi, G., Fläschner, D., Hodnebrog, Ø.,
493 Kasoar, M., Kharin, V., Kirkev\aag, A., Lamarque, J.-F., Mülmenstädt, J., Olivié, D., Richardson, T., Samset, B. H., Shindell, D., Stier, P.,
494 Takemura, T., Voulgarakis, A., and Watson-Parris, D.: Understanding Rapid Adjustments to Diverse Forcing Agents, Geophys. Res. Lett.,
495 45, 12,023–12,031, 2018.

496 Takahashi, T., Sutherland, S. C., Wanninkhof, R., Sweeney, C., Feely, R. A., Chipman, D. W., Hales, B., Friederich, G., Chavez, F.,
497 Sabine, C., Watson, A., Bakker, D. C. E., Schuster, U., Metzl, N., Yoshikawa-Inoue, H., Ishii, M., Midorikawa, T., Nojiri, Y., Körtzinger,
498 A., Steinhoff, T., Hoppema, M., Olafsson, J., Arnarson, T. S., Tilbrook, B., Johannessen, T., Olsen, A., Bellerby, R., Wong, C. S., Delille,
499 B., Bates, N. R., and de Baar, H. J. W.: Climatological mean and decadal change in surface ocean pCO2, and net sea–air CO2 flux over the
500 global oceans, Deep Sea Res. Part 2 Top. Stud. Oceanogr., 56, 554–577, 2009.

501 Tanaka, K., Kriegler, E., Bruckner, T., Hooss, G., Knorr, W., Raddatz, T. J., and Tol, R.: Aggregated carbon cycle, atmospheric chemistry,
502 and climate model (ACC2), Institute, Max Planck, Hamburg, 188 pp., 2007.

503 Thornton, P. E. and Rosenbloom, N. A.: Ecosystem model spin-up: Estimating steady state conditions in a coupled terrestrial carbon and
504 nitrogen cycle model, Ecol. Modell., 189, 25–48, 2005.

505 Vega-Westhoff, B., Sriver, R. L., Hartin, C. A., Wong, T. E., and Keller, K.: Impacts of observational constraints related to sea level on
506 estimates of climate sensitivity, Earths Future, 7, 677–690, 2019.

507 Wang, S., Zhang, Y., Ju, W., Chen, J. M., Ciais, P., Cescatti, A., Sardans, J., Janssens, I. A., Wu, M., Berry, J. A., Campbell, E.,
508 Fernández-Martínez, M., Alkama, R., Sitch, S., Friedlingstein, P., Smith, W. K., Yuan, W., He, W., Lombardozzi, D., Kautz, M., Zhu, D.,
509 Lienert, S., Kato, E., Poulter, B., Sanders, T. G. M., Krüger, I., Wang, R., Zeng, N., Tian, H., Vuichard, N., Jain, A. K., Wiltshire, A.,
510 Haverd, V., Goll, D. S., and Peñuelas, J.: Recent global decline of CO_2 fertilization effects on vegetation photosynthesis, Science, 370,
511 1295–1300, 2020.

512 Willner, S., Hartin, C., and Gieseke, R.: pyhector: A Python interface for the simple climate model Hector, J. Open Source Softw., 2, 248,
513 2017.

514 Winkler, K., Fuchs, R., Rounsevell, M., and Herold, M.: Global land use changes are four times greater than previously estimated, Nat.
515 Commun., 12, 2501, 2021.

516 Woodard, D. L., Shiklomanov, A. N., Kravitz, B., Hartin, C., and Bond-Lamberty, B.: A permafrost implementation in the simple carbon–
517 climate model Hector v.2.3pf, Geosci. Model Dev., 14, 4751–4767, 2021.

518 Yue, C., Ciais, P., Houghton, R. A., and Nassikas, A. A.: Contribution of land use to the interannual variability of the land carbon cycle,
519 Nat. Commun., 11, 3170, 2020.

520 Zeebe, R. E. and Wolf-Gladrow, D.: CO_2 in Seawater: Equilibrium, Kinetics, Isotopes, Gulf Professional Publishing, 346 pp., 2001.

521

522 **Table 1. Default Hector parameter values and their sources.** The parameter name column is the name as it appears in the
523 model's ini (initialization) files. This is not an exhaustive table of Hector parameters but rather contains the parameters that
524 have been updated since Hartin et al. (2015). For a complete collection of parameter values and their sources, refer to the
525 default initialization files available at https://github.com/JGCRI/hector/tree/main/inst/input. Preindustrial values here are
526 assumed to be circa 1745, the start of a Hector run.

Parameter	Description	Value	Units	Source
CH4N	Natural CH_4 Emissions are assumed to be constant over the historical and future period	338	Tg CH_4 yr^{-1}	See section 2.2.6 for details
N2ON	Natural N_2O emissions, assumed to be constant of the historical and future period	9.7	Tg N yr^{-1}	
beta	CO_2 fertilization factor (β) (increase in NPP productivity with increasing CO_2 concentrations)	0.55	unitless	
q10_rh	Heterotrophic respiration temperature sensitivity factor (Q_{10})	2.2	unitless	
diff	Vertical ocean heat diffusivity (κ), the rate of heat diffuses into the ocean	1.16	cm^2/s	
preind_surface_c	Initial size of the preindustrial surface ocean carbon pool	900	Pg C	Figure 5.12 (Canadell et al., 2021)
preind_interdeep_c	Initial size of the preindustrial intermediate and deep ocean carbon pool	37100	Pg C	
C0	Preindustrial CO_2 concentration	277.15	ppmv CO_2	Table 7.SM.1 (Smith et al., 2021)
N0	Preindustrial N_2O concentration	273.87	ppbv N_2O	
M0	Preindustrial CH_4 concentration	731.41	ppbv CH_4	
npp_flux0	Preindustrial net primary production	56.2	Pg C yr^{-1}	Ito (2011)
TOS0	Mean preindustrial absolute ocean air temperature	18	°C	

					From processed CMIP6 data (Pressburger and Dorheim, 2022)
deltaHL0	Difference between high latitude preindustrial ocean temp and TOS0	-16.4	°C		
deltaLL0	Difference between low latitude preindustrial ocean temp and TOS0	2.9	°C		

527

528 **Table 2: Descriptions and summaries of the Hector constraints.** The constraint name column reflects the name as it
529 appears in the model's ini (initialization) files.

Name	Description	Implementation
CO2_constrain	Time series of CO_2 concentration values (ppmv CO_2)	CO_2 radiative forcing (RF) is calculated from the user-provided CO_2 concentrations and then used to calculate total RF and temperature. If needed, CO_2 is debited/credited to/from the deep ocean to meet the CO_2 concentration constraint and satisfy Hector's global carbon cycle mass balance check.
CH4_constrain	Time series of CH_4 concentration values (ppbv CH_4)	CH_4 RF is calculated from the user-provided CH_4 concentrations, feeding into total RF and temperature.
N2O_constrain	Time series of N_2O concentration values (ppbv N_2O)	N_2O RF is calculated from the user-provided N_2O concentrations.
X_constrain (X is the identifier for one of 26 halocarbons modeled by Hector)	Time series for a single halocarbon concentration (pptv)	RF for halocarbon X is calculated from the user-provided concentrations.
RF_tot_constrain	Time series of total radiative forcing value (W m^{-2})	User-provided total RF values are used to calculate temperature and heat flux. In this case, the emission inputs do not drive model behavior.
NBP_constrain	Time series of Net Biome Production values (Pg C yr^{-1})	User-provided NBP values are used to up/downscale NPP and RH so that their total matches the constraint. This effectively bypasses the model's terrestrial carbon cycle.
tas_constrain	Time series of global mean air temperature values (°C)	User-provided temperature values overwrite Hector's, with a smooth transition between the constrained and free-running behavior.

530 **Table 3. Key emergent climate metrics, historical warming, effective radiative forcing, and future warming from**
531 **Hector versus the IPCC AR6 'best estimates' from the AR6 Table 7.SM.4.** The Hector values were generated from runs
532 using Hector's default parameterization in the free-running emission-driven mode for historical and SSP scenarios. The
533 parenthetical IPCC AR6 values indicate the AR6 'very likely' (5-95)% ranges. Acronyms include equilibrium climate
534 sensitivity (ECS), transient climate response to cumulative carbon emissions (TCRE), transient climate response (TCR),
535 global surface air temperature (GSAT), and effective radiative forcing (ERF) (Nijsse et al., 2020).

Key Metrics		Hector	IPCC AR6
ECS (°C)		3	3 (2, 5)
TCRE (°C per 1000 GtC)		1.51	1.65 (1, 2.3)
TCR (°C)		1.84	1.8 (1.2, 2.4)
Historical Warming and Effective Radiative Forcing			
GSAT Warming (°C, 1995-2014 relative to 1850-1900)		0.73	0.85 (0.67, 0.98)
Ocean heat content change (ZJ, 1971-2018)		471	396 (329, 463)
Total Aerosol ERF (W m^{-2}, 2005-2015 relative to 1750)		-1.24	-1.3 (-2, -0.6)
WMGHG ERF (W m^{-2}, 2019 relative to 1750)		3.87	3.32 (3.03, 3.61)
Methane ERF (W m^{-2}, 2019 relative to 1750)		0.54	0.54 (0.43, 0.65)
Future Warming (GSAT, °C relative to 1995-2014)			
SSP1-1.19	2021-2040	0.73	0.61 (0.38, 0.85)
	2041-2060	0.90	0.71 (0.4, 1.07)
	2081-2100	0.72	0.56 (0.24, 0.96)
SSP1-2.6	2021-2040	0.75	0.63 (0.41, 0.89)

	2041-2060	1.08	0.88 (0.54, 1.32)
	2081-2100	1.10	0.90 (0.51, 1.48)
SSP2-4.5	2021-2040	0.75	0.66 (0.44, 0.90)
	2041-2060	1.29	1.12 (0.78, 1.57)
	2081-2100	1.98	1.81 (1.24, 2.59)
SSP3-7.0	2021-2040	0.76	0.67 (0.45, 0.92)
	2041-2060	1.43	1.28 (0.92, 1.75)
	2081-2100	2.94	2.76 (2.00, 3.75)
SSP5-8.5	2021-2040	0.88	0.76 (0.51, 1.04)
	2041-2060	1.74	1.54 (1.08, 2.08)
	2081-2100	3.79	3.50 (2.44, 4.82)

536

537

Figure 1. Conceptual diagram of the CO$_2$ fluxes (numbered thick gray arrows) between Hector's four major carbon cycle boxes: a well-mixed atmosphere (Atmosphere), terrestrial carbon cycle (Land), ocean carbon cycle (Ocean), and geological fossil fuel reservoir (Earth). The thinner arrows within the land and ocean boxes allude to Hector's more complex submodule carbon cycle dynamics, which are not discussed in detail here. The solid lines indicate that CO$_2$ fluxes are calculated within Hector, whereas the dashed lines indicate that the fluxes are externally defined inputs read into the model; two-headed arrows imply a potential two-way exchange of carbon. The fluxes are: (1) CO$_2$ emissions from fossil fuels and industry and uptake of carbon capture technologies; (2) CO$_2$ emissions and uptake from land use change (e.g., afforestation, deforestation, etc.); (3) vegetation uptake from the atmosphere (4) the aggregate CO$_2$ from respiration from the terrestrial biosphere; and ocean carbon (5) uptake and (6) outgassing. The model's permafrost implementation (Woodard et al., 2021) emits both CO$_2$ and CH$_4$ into the atmosphere from its "Thawed Soil" pool, whereas the "Soil" pool emits only heterotrophic CO$_2$ respiration.
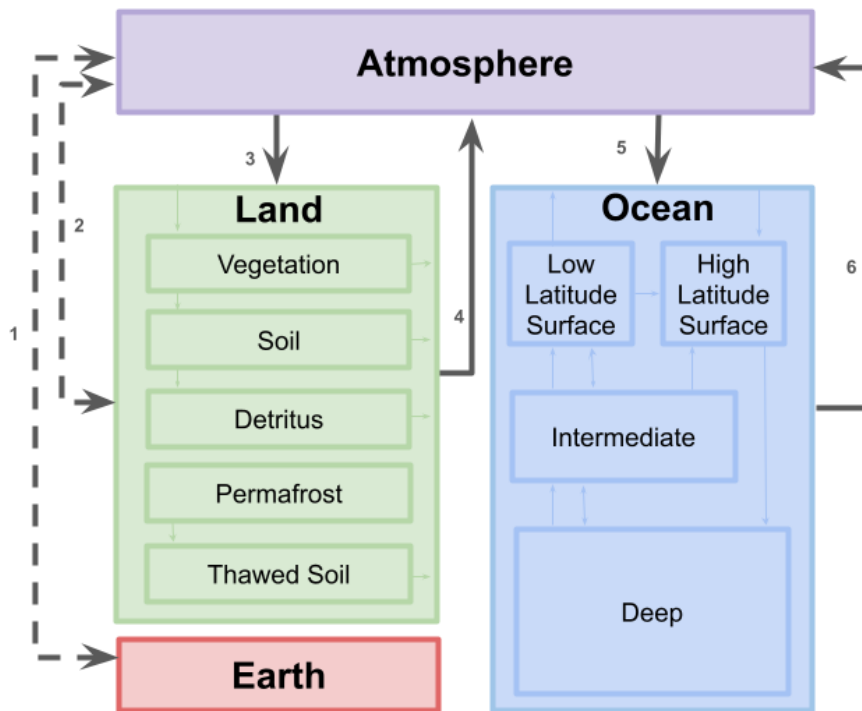
553   **Figure 2. Hector CO₂ concentrations (orange) compared with the CMIP6** (Meinshausen et al., 2017) **CO₂**

554   **concentrations observational product (black)**
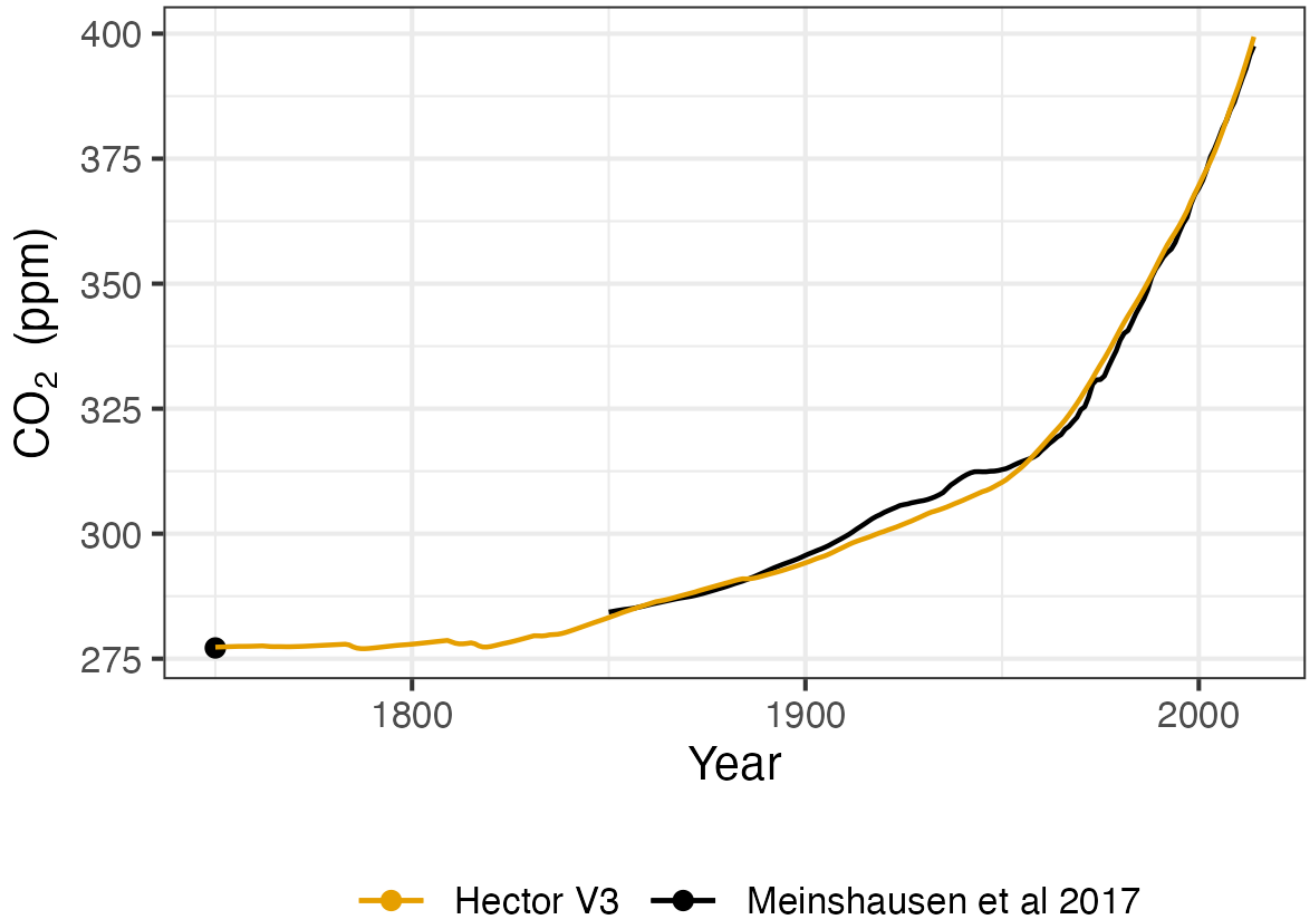
555

556

557 **Figure 3. Global mean surface temperature anomaly relative to 1951-1980 for Hector (orange) and HadCRUT 5**

558 **global mean surface temperature observations** (Morice et al., 2021) **(black, with associated uncertainty). The inset**

559 **figure shows the rolling decadal average.**
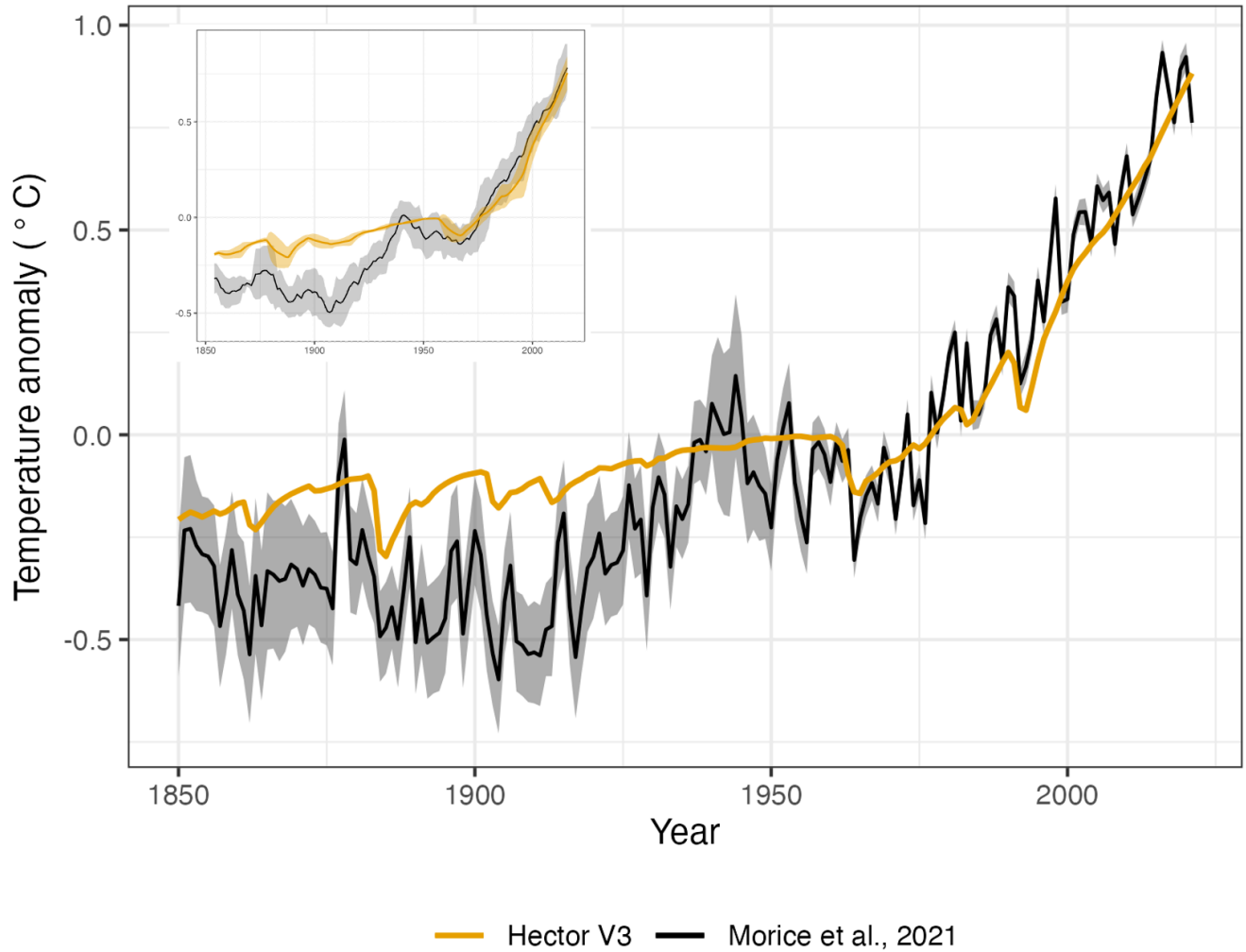
560

561

562 **Figure 4. Global, land, and sea surface temperature anomalies relative to 1850-1900 from concentration-driven**

563 **("constrained") Hector, in orange, and temperature output from 15 different CMIP6-participating ESMs, in grey**

564 **(see Supplementary Table 8).**

565

566
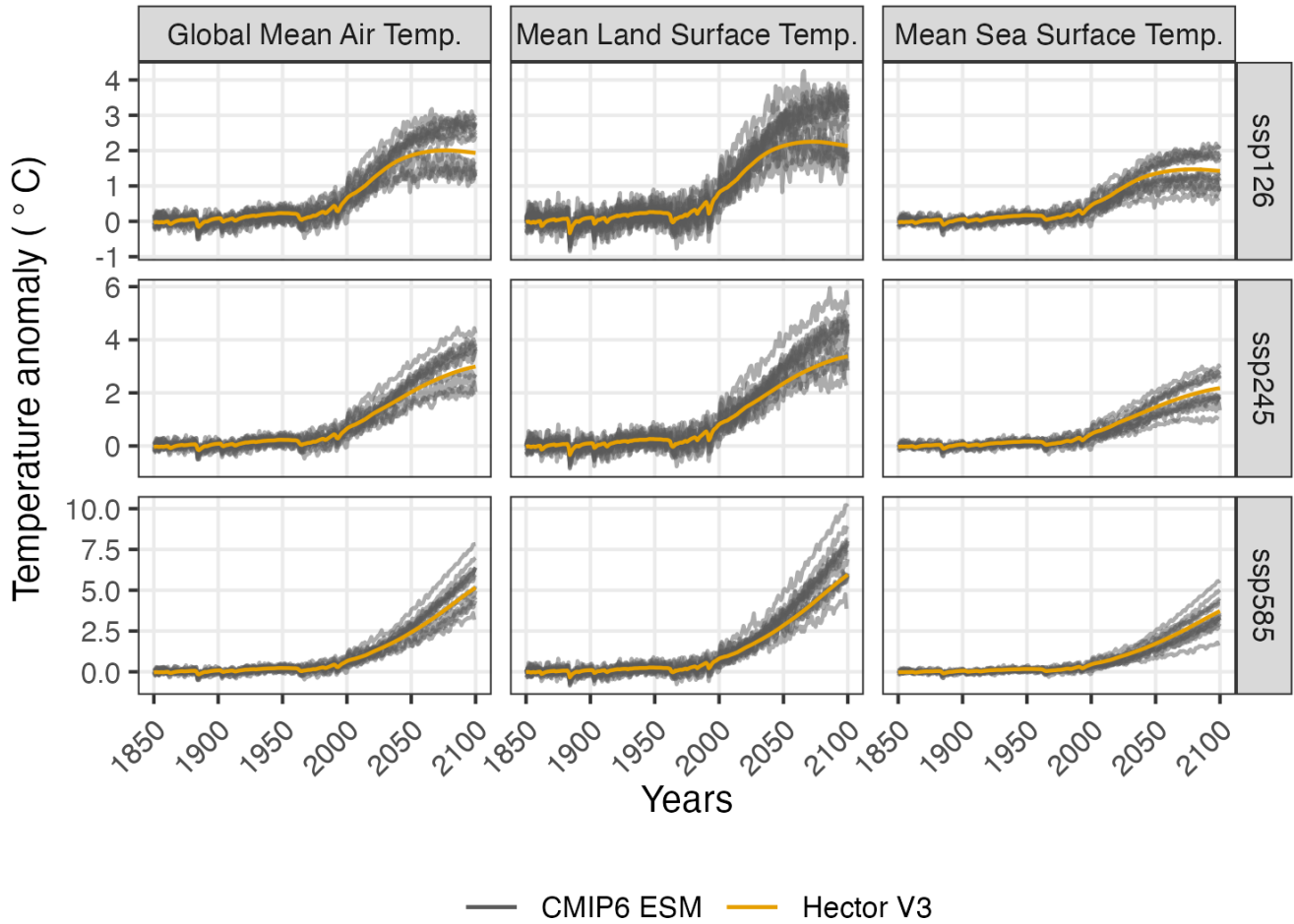
Figure 5. Global temperature anomaly from 1% CO₂ and 4xCO₂ stylized experiments (Eyring et al., 2016) **for Hector**

(orange) and 15 different CMIP6 participating ESMs (grey lines; see Supplementary Table 8).

569